

Article

Characterization of Ground Thermal Conditions for Shallow Geothermal Exploitation in the Central North China Plain (NCP) Area

Wanli Wang ^{1,2} , Guiling Wang ^{1,2}, Feng Liu ^{1,2} and Chunlei Liu ^{1,2,*}

¹ Institute of Hydrogeology and Environmental Geology, Chinese Academy of Geological Sciences, Shijiazhuang 050061, China

² Technology Innovation Center for Geothermal & Hot Dry Rock Exploration and Development, Ministry of Natural Resources, Shijiazhuang 050061, China

* Correspondence: liuchunlei@mail.cgs.gov.cn

Abstract: The central North China Plain (NCP) is one of the rapidly developing regions in China which has a great potential for ground source heat pump (GSHP) system applications. However, the ground thermal property, which is a prerequisite for GSHP system design, has been insufficiently investigated. In this paper, the ground thermal conditions including ground temperature and thermal conductivity are characterized in three representative hydrogeological regions in the NCP area: the piedmont alluvial plain, the central alluvial plain, and the coastal plain. Results show that the geothermal gradient below 40 m in depth in this area ranges from 0.018 °C/m to 0.029 °C/m. Although the thermal conductivity measured by soil samples differs slightly among the three regions, parameters in the piedmont plain have a larger variability than in the central and coastal plain due to the significant heterogeneity of the lithology. Thermal conductivity measured by the thermal response test (TRT) ranges between 2.37 and 2.68 W/(m·K) in the piedmont plain and varies between 1.35 and 1.94 W/(m·K) in the central and coastal plain, indicating that the piedmont plain has a higher potential for shallow geothermal exploitation than other two sub-areas. Comparing the TRT with laboratory measurements, the thermal conductivity obtained by the TRT is greater than that of the lab measurements in the piedmont plain due to the TRT outputs including the effects of groundwater flow. Therefore, the TRT is highly recommended to estimate the effective thermal conductivity of the ground in the piedmont plain, while laboratory and field tests are both suitable methods for the determination of thermal conductivity in the central and coastal plains.

Keywords: ground source heat pump systems (GSHPs); thermal conductivity; hydrogeological settings; thermal response test (TRT); constant heating-temperature method (CHTM); the center North China Plain (NCP)



Citation: Wang, W.; Wang, G.; Liu, F.; Liu, C. Characterization of Ground Thermal Conditions for Shallow Geothermal Exploitation in the Central North China Plain (NCP) Area. *Energies* **2022**, *15*, 7375. <https://doi.org/10.3390/en15197375>

Academic Editor: Javier F. Urchueguía

Received: 23 August 2022

Accepted: 6 October 2022

Published: 8 October 2022

Publisher's Note: MDPI stays neutral with regard to jurisdictional claims in published maps and institutional affiliations.



Copyright: © 2022 by the authors. Licensee MDPI, Basel, Switzerland. This article is an open access article distributed under the terms and conditions of the Creative Commons Attribution (CC BY) license (<https://creativecommons.org/licenses/by/4.0/>).

1. Introduction

Due to the energy-saving, high efficiency, and environmental friendliness [1,2] advantages, ground source heat pump systems (GSHPs) have developed rapidly in recent years [3]. Up to the year 2019, the installed capacity of GSHPs accounted for 71.6% of the global total installed capacity of geothermal energy utilization [4]. The North China Plain (NCP), which is a major economic center of China, is one of the regions with abundant geothermal energy. Based on investigations of the geothermal resources in the shallow ground of the major cities of the NCP, it has been shown that shallow geothermal energy can satisfy the space heating and cooling for an area of 1600–3500 km² [5]. Up to the year 2015, a total building area of 85 km² for both heating and cooling has been installed in the main cities of the NCP. However, for rural areas of the NCP, inefficient bulk coal has been commonly utilized for space heating as a centralized heating system was not available, causing air pollution in the winter [6,7]. Therefore, clean energy such as geothermal energy

is preferentially recommended for these areas. Although the hydrogeologic conditions of the NCP are well studied, the understanding of the main controls affecting the efficiency of GSHP systems in the NCP is limited.

In GSHPs, the depth of a borehole typically varies from 40 to 200 m [1], and the heat is transferred from the ground to a building by coupling a ground heat exchanger and heat pumps [8]. In a specific borehole, the efficiency of GSHP systems is influenced by the temperature and thermal conductivity of the ground [9,10]. By using temperature sensors along the borehole, ground temperature data can be obtained for different times and depths [11]. Meanwhile, these sensors can be used as monitoring points during the operation of GSHPs. The accuracy of the data depends on the precision of the temperature sensors. However, thermal conductivity representative of the subsurface medium during utilization is difficult to obtain. In recent years, the problem of performance declines after a long-term operation has occurred in the NCP [3], largely due to the limited availability of ground thermal properties. Therefore, the characterization of ground thermal properties is critical to the sustainability of GSHP systems.

Thermal conductivity measurements of the subsurface media can be undertaken by laboratory and field methods [12,13]. In the laboratory, steady-state and transient methods are commonly applied to measure the thermal conductivity of samples [14]. For unconsolidated sediments, a needle source probe is generally adopted in the laboratory. The thermal conductivity of sediments is closely related to factors such as water content, density, and mineralogical composition [15–17]. By measuring numerous samples from the borehole, the relations between thermal conductivity and these factors can be analyzed.

However, the initial conditions of borehole samples are not easy to maintain, and the laboratory method does not take into account the effect of groundwater flow, both of which have a significant impact on the determination of thermal conductivity [18]. Therefore, it is necessary to combine field methods with laboratory measurements to determine the thermal conductivity of subsurface media. A thermal response test (TRT) is a common method to determine the thermal-physical parameters of boreholes such as the effective ground conductivity and effective thermal resistance [19].

For a conventional TRT, a constant heat load of water is injected and circulated through the U-pipe of a borehole heat exchange (BHE) buried in the ground. Parameters such as the inlet and outlet fluid temperature of the U-pipe and flow rate should be measured continuously. In the preliminary phase of a TRT, when circulating the fluid inside the pipe loops without heat injection or extraction, the undisturbed ground temperature can be estimated by averaging the recording inlet and outlet fluid temperature when a thermal equilibrium has been reached between the fluid inside the pipes and the ground [20]. The accuracy of the measurement, thermal insulation of the equipment, and the heat added to the circulating fluid due to the pump work affect the accuracy of the test [21].

The effective ground conductivity and effective thermal resistance can then be estimated through analytical or numerical models with the measuring outputs of the TRT. Although the conventional TRT is widely used, this method cannot adequately consider the effects of the stratified ground and the groundwater flow [22]. Some improved methods have been proposed in recent years [23]. Franco and Conti (2020) have reviewed and discussed different TRT methods including the distributed thermal response test (DTRT) [24], enhanced thermal response test (ETRT) [25], and constant heating temperature method (CHTM) [26]. The DTRT and ETRT techniques can provide the ground conductivity of different geological layers and the groundwater influence can also be considered. The application of CHTM is able to simulate the actual operating conditions under both injection and extraction modes, showing that it can accurately reflect the thermal properties of the ground and the thermal performance of BHEs [26,27].

In this study, the ground thermal properties of the central NCP are determined in three representative hydrogeological regions: the piedmont alluvial plain, the central alluvial plain, and the coastal plain. Temperature sensors were installed at different depths to obtain ground temperature profiles in the typical boreholes of nine cities located in these regions,

and CHTM-based TRTs were performed to estimate the effective thermal conductivity and were then compared with laboratory measurements to better understand the effects of the groundwater flow.

2. Materials and Methods

2.1. Hydrogeological Settings

The NCP is one of the largest plains in east Asia, covering an area of 140,000 km² [28]. Cities such as Baoding (BD), Shijiazhuang (SJZ), Hengshui (HS), Renqiu (RQ), Wuqiao (WQ), Hejian (HJ), Cangzhou (CZ), Qingxian (QX) and Huanghua (HH) are in the center of the NCP. The average annual temperature of this area ranges from 12 to 13 °C and the average annual precipitation ranges from 500 to 600 m [29]. The center of the NCP is bounded by Taihang Mountain to the west and Bohai Bay to the east [30]. The whole region can be divided into the piedmont alluvial plain (I), the central alluvial plain (II), and the coastal plain (III) from the west to the east [31–33] (Figure 1). The cross-section A-A' (shown in Figure 1), which crosses through the three different hydrogeological units, has been widely used in studies on groundwater circulation and the evolution of the NCP [28,29,33–36]. Based on abundant borehole data, Figure 2 summarizes the distribution of Quaternary aquifer units and the pattern of groundwater flow along the cross-section.

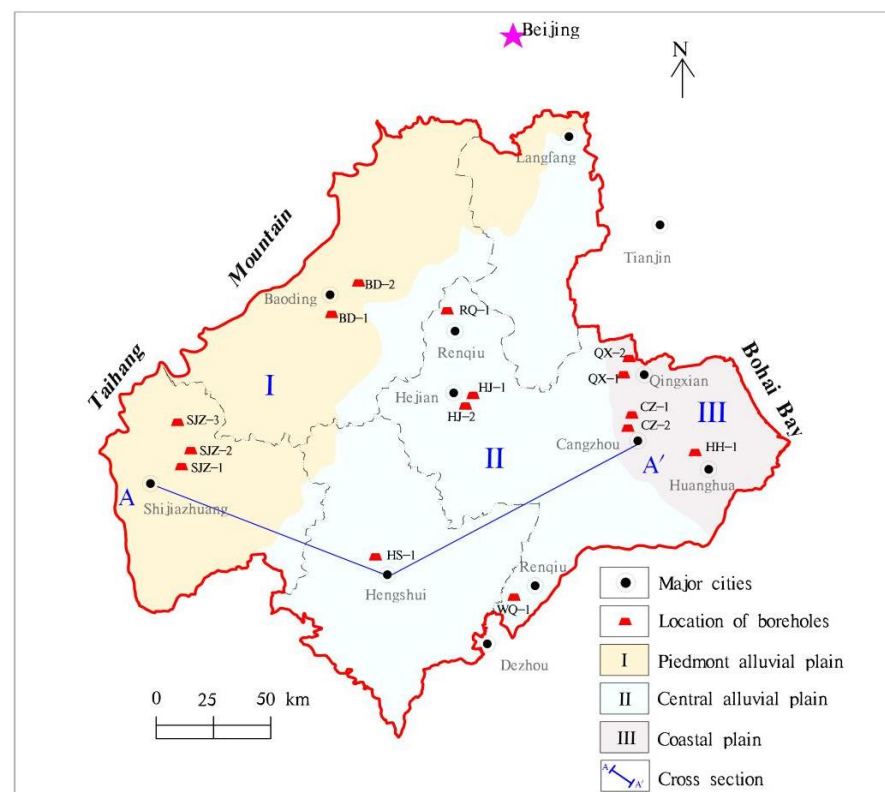


Figure 1. Map of the central North China Plain.

General features of the representative regions are shown in Table 1. For the piedmont alluvial plain, the Quaternary sediments within 200 m are dominated by sand, gravel, and clay with great inhomogeneity [36]. The Quaternary aquifer is unconfined and is recharged by infiltration of atmospheric precipitation and lateral flow from mountains. With a relatively high hydraulic conductivity and high specific yield, groundwater flow velocity in this region ranges between 0.013 and 0.26 m/d [36] and the water table depth ranges between 20 and 45 m [37]. The cities of BD and SJZ are representative cities of this region.

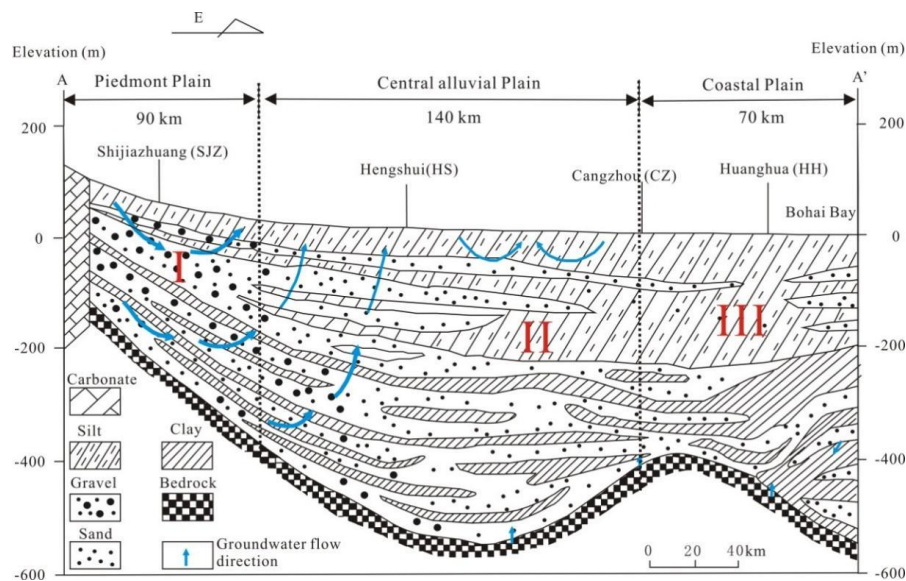


Figure 2. Conceptual cross-section along the A-A' line (modified after [28,33,36]).

Table 1. General features of the representative regions.

Hydrogeological Setting	Representative Region	Water Table Depth (m)	Groundwater Flow Velocity (m/d)	Lithology (<150 m)
Piedmont Plain (I)	BD and SJZ	20–45	0.013–0.26	Gravel, sand, silt, and clay
Central Plain (II)	HS, RQ, HJ, and WQ	3–5	0.002–0.10	Clay, silty clay, and silt
Coastal plain (III)	CZ, QX, and HH	1–5	0.002–0.10	Silt and silty clay

HS, RQ, HJ, and WQ are situated in the central alluvial plain, and the Quaternary sediments within 200 m are dominated by silt and clay deposits [34]. With lithology changing to finer deposits, the Quaternary aquifers become semi-confined and confined [28]. Compared with the piedmont alluvial plain, both permeability and groundwater flow velocity decrease dramatically. The flow velocity varies between 0.002 and 0.10 m/d in this region [35,36] and the water table depth generally ranges between 3 and 5 m [37].

CZ, QX, and HH are situated on the coastal plain, and the marine and alluvial sediments are dominated by silt, sandy clay, and silty clay [35,36]. Along the eastward hydraulic gradient, the sediment particles become finer and the clay appears interbedded [33], which could lead to lower hydraulic conductivity and flow velocity. In this region, the water table depth is always shallower than 5 m [37,38].

2.2. Test Sits and Borehole Setting

In the current study, 15 boreholes were drilled within the three representative regions. Among them, 5 boreholes are in BD and SJZ cities, representing the piedmont alluvial plain (I), 5 boreholes are in RQ, HJ, WQ, and HS cities, representing the central alluvial plain (II), and 5 boreholes are in HH, QX and CZ cities, representing the coastal plain (III) (Figure 1). Because the boreholes are used for shallow geothermal energy, the depth of all boreholes is within 150 m.

Before conducting the relevant tests, hydrogeological investigations were carried out in the study area to obtain the groundwater level of the wells and then the water-level contour map of the area was plotted. Following this, the hydraulic gradient was obtained and, combined with the permeability of the aquifer, the groundwater flow velocity was estimated at each borehole location. Detailed information on the 15 boreholes is shown in Table 2.

Table 2. Borehole and equipment installation details.

Hydrogeological Setting	Borehole	Depth (m)	Water Table Depth (m)	Groundwater Flow Velocity (m/d)	Temperature Sensor
Piedmont plain (I)	BD-1	100	25	0.085	✓
	BD-2	100	15	0.04	✓
	SJZ-1	100	45	0.138	
	SJZ-2	120	42	0.1162	✓
	SJZ-3	120	38	0.2125	✓
Central plain (II)	RQ-1	120	5	0.005	✓
	HJ-1	150	5	<0.005	
	HJ-2	120	5	<0.005	✓
	WQ-1	120	5	0.005	✓
	HS-1	100	5	0.005	
Coastal plain (III)	CZ-1	100	4	0.005	
	CZ-2	120	4	<0.005	
	HH-1	150	3	<0.005	✓
	QX-1	120	3	<0.005	
	QX-2	120	3	<0.005	✓

Sediments of boreholes in BD and SJZ have coarse particle sizes, such as gravel, coarse sand, and medium sand, while sediments of boreholes in other cities have a relatively finer particle size of silt and silty clay. Soil samples were collected every 5 m at each borehole and then covered by a plastic membrane to prevent moisture loss before sending to the laboratory. Texture, bulk density, water content, and thermo-physical properties were analyzed by the Hebei University of Technology.

The thermal conductivity of soil samples was measured by a KD2 device (Decagon Devices, Pullman, WA, USA) in line with ASTM Standard D5334-00. This device follows the principle of an infinite line heat source, and the sample should have a certain thickness to avoid boundary effects during the test. When the temperature of the heat source ranges between 5 and 40 °C, the device has 5% accuracy [39]. The samples were tested as soon as possible after being sent to the laboratory to maintain the original humidity and were tested under natural pressure.

After drilling was completed, a DN32 double-U-shaped BHE was installed into the borehole. In order to reduce the test measurement error, the length of the above-ground section of the BHE was retained for about 1 m and insulated to minimize heat loss. For long-term monitoring of the ground temperature, calibrated PT1000-type temperature sensors with 0.1 °C accuracies were installed at different depths of the outside of the U-pipes and buried in the borehole. In addition, a data acquisition recorder was used to collect temperature distributions at 10 min intervals. For financial considerations, only 2–4 boreholes were selected in each hydrogeological setting. The temperature sensors were equipped at 5 m intervals within 50 m of depth, and at 10 m intervals when deeper than 50 m.

2.3. Thermal Response Test and Parameters Estimation

For a CHTM-based TRT, a constant temperature is injected into or extracted from the ground. The CHTM-based TRT equipment is very similar to conventional test equipment except that the temperature of the inlet fluid is controlled by regulating the heating and cooling device [26]. Parameters such as inlet fluid temperature (T_{in}), outlet fluid temperature (T_{out}), and fluid flow rate were measured simultaneously. The temperature is measured by a Pt1000 type platinum resistance with a measurement accuracy of 0.1 °C and the flow rate is measured by an electromagnetic-type flow meter with 0.001 m³/h accuracy. Before the test, all sensors were calibrated in the thermal engineering laboratory of the Hebei University of Technology to ensure the validity of the data. The pipes connecting the test equipment to the BHE must be well insulated to prevent energy loss.

During tests, the mean fluid temperature (T_f) (i.e., the average temperature of the inlet and outlet fluid) can be formulated by the Fourier equation:

$$T_f - T_b = q R_b \quad (1)$$

where T_f is the mean fluid temperature ($^{\circ}\text{C}$), $T_f = (T_{in} + T_{out})/2$, T_b is the temperature of the borehole wall ($^{\circ}\text{C}$), q is the heat transfer rate of BHEs (W/m), and R_b is the borehole effective thermal resistance ($(\text{m}\cdot\text{K})/\text{W}$).

With

$$q = \frac{m c_p (T_{in} - T_{out})}{H} \quad (2)$$

where m is the flow rate (kg/s), c_p is the heat capacity of the fluid ($\text{J}/\text{kg}/\text{K}$), and H is the length of the borehole (m).

The G-function is induced to solve the heat transfer outside the borehole and can be described as [40]:

$$T_b - T_0 = \frac{q}{2\pi\lambda} G(t) \quad (3)$$

where T_0 is the undisturbed ground temperature ($^{\circ}\text{C}$), t is time (s), and λ is the ground effective thermal conductivity $\text{W}/(\text{m}\cdot\text{K})$.

Lamarche and Beauchamp [41] proposed a simplified form of the integral transform which was applied to the G-function. During tests, the heat flux in the BHE varies until it reaches a steady state. However, the traditional analytical line-source model (LM) ignores the heat transfer process inside the borehole which does not correspond to the practical situation. Thus, the cylindrical-source model (CSM) was applied for the interpretation.

The relation between the mean fluid temperature T_f and the steady state heat transfer rate of BHEs q should be linear under different inlet temperatures of the BHE and makes it possible to obtain the slope K . Combining Equations (1)–(3), the ground effective thermal conductivity can be obtained by [26]:

$$\lambda = \frac{G K}{2\pi(1 - KR_b)} \quad (4)$$

The determination of G-functions is a major approach for CSM to analyze the heat-transfer behavior between the BHE and its surrounding soils. In order to solve the analytical model including G-functions, a computer program was developed by Wang [26] using Visual Basic 6.0 (Microsoft, Redmond, WA, USA).

The test procedure of every borehole usually contains two stages [26]. First, the undisturbed ground temperature is measured for 20–48 h under normal conditions without heating or cooling, until the inlet and outlet fluid temperature of the BHE reached a steady state. The second stage is the heat-extraction/injection modes with the constant inlet fluid temperature. The inlet temperature ranged from 5 to 8 $^{\circ}\text{C}$ for the heat-extraction mode and from 19 to 35 $^{\circ}\text{C}$ for the heat-injection mode. These stages of the CHTM-based TRTs of 15 boreholes including time duration (Δt) and inlet fluid temperature (T_{in}) in different boreholes are presented in Table 3.

Table 3. Data related to the conducted CHTM-based TRT of all boreholes.

Hydrogeological Setting	Borehole	Steady Stage	Heat-Extraction Stage		Heat-Injection Stage	
		Δt (h)	Δt (h)	T_{in} ($^{\circ}\text{C}$)	Δt (h)	T_{in} ($^{\circ}\text{C}$)
Piedmont plain (I)	BD-1	24	48	7.41	48	31.61
	BD-2	26	30	5.38	26	29.23
	SJZ-1	23	/	/	48	32.19
	SJZ-2	24	/	/	48	33.00
	SJZ-3	26	/	/	24	19.08
Central plain (II)	RQ-1	24	24	8.45	20	29.07
	HJ-1	18	24	9.75	21	28.92
	HJ-2	18	24	8.26	24	30.00
	WQ-1	21	23	8.53	23	30.21
	HS-1	48	48	7.83	48	30.20
Coastal plain (III)	CZ-1	48	48	7.48	48	29.65
	CZ-2	48	48	8.00	48	30.00
	HH-1	24	/	/	48	25.47
	QX-1	24	/	/	48	29.87
	QX-2	24	/	/	48	25.90

3. Results and Discussions

3.1. Ground Temperature

The borehole temperatures of nine boreholes were first collected. Figure 3 presents the ground temperature profiles of these boreholes.

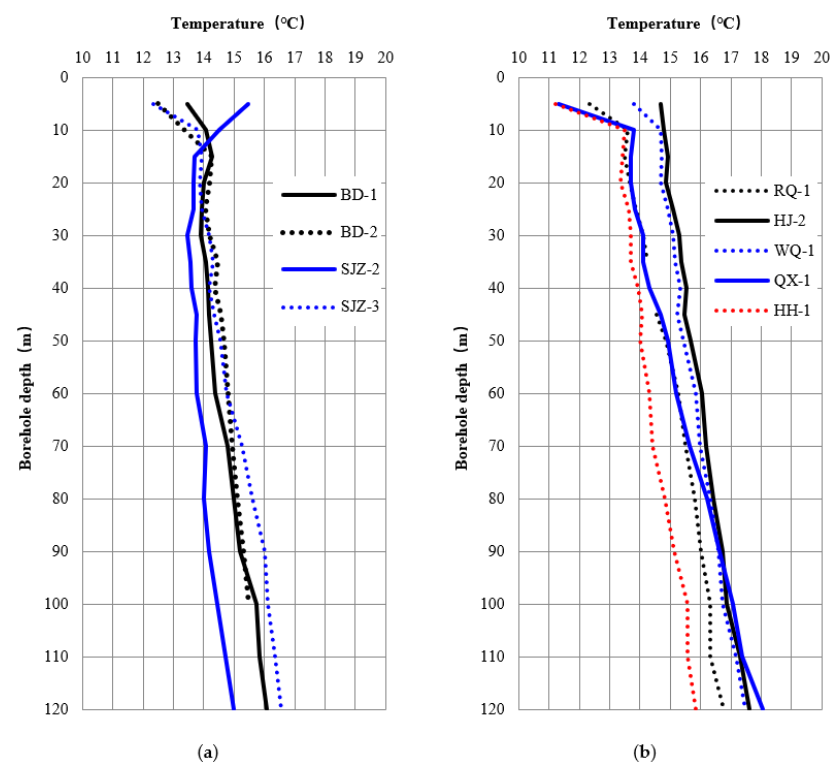


Figure 3. Undisturbed ground temperature profile: (a) the piedmont plain; (b) the central and coastal plain.

The temperature profiles of the nine boreholes show a similar tendency and three temperature sections can be distinguished: (1) a shallow section (including the surface part), where the ground temperature is mostly affected by climatic conditions, including air temperature, solar radiation, etc., (2) a constant-temperature section, where the ground tem-

perature is relatively stable and is similar to the average surface ground temperature [42], and (3) a deep section, where the temperature increases with depth and the slope of the curve called geothermal gradient. This phenomenon is identical to other previous research areas [27,43,44].

In the four typical boreholes at the piedmont plain, the ground temperature within the 15 m depth is highly influenced by seasonal atmospheric conditions and the influence reduces as the depth increases (Figure 3a). The middle section between 15 m and 40 m has a relatively constant ground temperature which ranges from 13.59 °C in SJZ-2 and 14.27 °C in BD-2. The temperature gradient in North China normally ranges from 0.02–0.03 °C/m [7]. For boreholes BD-1 and SJZ-3, the deep section below 40 m in depth has normal temperature gradients of 2.45 and 2.87, while for boreholes SJZ-2 and BD-2, the temperature gradients are only 0.018 °C/m and 0.019 °C/m, respectively, which are lower than the normal range. Table 4 lists the main lithology of borehole SJZ-2. The gravel layer (fine sand, coarse sand, and gravel) covers 58% of the layer thickness. Especially for depths from 47 m to 93 m, the ground is dominated by coarse sand and gravel which has a relatively strong groundwater flow and high hydraulic conductivity. The ground temperature rises slowly compared to other boreholes due to the strong cooling effect of groundwater flow on the surrounding ground [27]. For the deep section, the ground temperature is dominated by convection instead of conduction which leads to a lower gradient [21,27,45]. The same phenomenon occurred in borehole BD-2.

Table 4. The sedimentary sequence of rock formations of borehole SJZ-2.

Depth (m)	Thickness (m)	Lithology
14	14	clay, silty clay, and silt
18	4	coarse sand
47	29	sandy clay
50	3	coarse sand
55	5	sandy clay
65	10	coarse sand
66	1	gravel
71	5	fine sand
77	6	gravel
93	16	coarse sand
120	27	fine sand and sandy clay interlayer
14	14	clay, silty clay, and silt
18	4	coarse sand
47	29	sandy clay
50	3	coarse sand
55	5	sandy clay

RQ-1, HJ-2, and WQ-1 are three boreholes located in RQ, HJ, and WQ in the central alluvial plain (Figure 3b). The ground temperature within the 10 m depth is influenced by the external environment. Between 10 m and 35 m in depth, the ground temperature keeps almost constant at 13.83 °C in RQ-1, 15.05 in HJ-2, and 14.87 °C in WQ-1. The temperature rises with an increase in depth, and the geothermal gradient is 0.026–0.029 °C/m, which is within the regular range of 0.02–0.03 °C/m in the NCP. Compared with borehole temperature profiles in the piedmont region, the central plain shows little effect from groundwater flow, which agrees with the finding of [27] that there is low horizontal groundwater velocity under the central and coastal plains.

For boreholes QX-1 and HH-1 located in the coastal plain, the shallow temperature layer presents seasonal variations up to a depth of 10 m (Figure 3b), which is similar to the temperature tendency of boreholes in the central alluvial plain. Between 10 m and 35 m in depth, the ground temperature keeps almost constant at 13.88 °C and 13.56 °C. Under this depth, the temperature rises with depth and the geothermal gradient is 0.025 °C/m.

3.2. Thermos-Physical Properties of the Geological Materials

To obtain the ground thermal properties, soil samples were collected every 5 m along a borehole, which leads to a total of 352 samples from the 15 boreholes. These samples include silty clay, silt, fine sand, silty-fine sand, medium-coarse sand, and coarse sand. The thermal conductivity of soil samples was measured by a KD2 device (Decagon Devices, USA) with a transient line heat source. Figure 4 shows the thermal conductivity of the soil samples at different depths of the 15 boreholes.

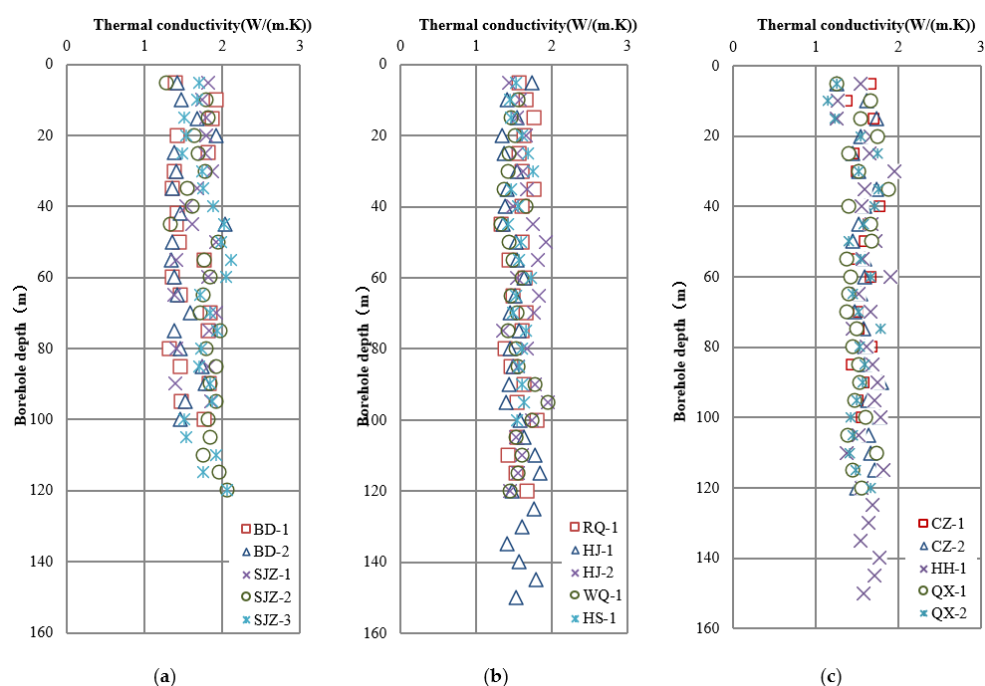


Figure 4. Vertical distribution of the thermal conductivity of locations in different regions: (a) the piedmont plain; (b) the central plain; and (c) the coastal plain.

The minimum, maximum, and the standard deviation of the thermal conductivity of the 15 boreholes were then calculated and listed in Table 5. The thermal conductivity of boreholes in the piedmont plain ranges from 1.28 to 2.11 W/(m·K), with a standard deviation varying between 0.62 and 0.89. For the central alluvial plain, this value ranges from 1.33 to 1.95 W/(m·K), with a standard deviation varying between 0.16 and 0.56. For the coastal plain, the thermal conductivity ranges from 1.14 to 1.95 W/(m·K), with a standard deviation varying between 0.21 and 0.69. Thermal conductivity in the piedmont plain exhibits a larger variability than that of the central and coastal plain due to the significant heterogeneity of the lithology. As mentioned in Section 2.1, the Quaternary sediments within 200 m depth in the piedmont plain are dominated by sand, gravel, and clay with great inhomogeneity, however, the Quaternary sediments within 200 m are dominated by fine-grained deposits of silt and clay materials.

The laboratory mean thermal conductivity of each borehole was obtained by the arithmetic mean method and listed in Table 5. It was found that the five boreholes in the piedmont plain have an average thermal conductivity varying between 1.53 and 1.79 W/(m·K). The six boreholes in the central alluvial plain have an average thermal conductivity varying between 1.54 and 1.64 W/(m·K), and the four boreholes in the coastal plain have an average thermal conductivity varying between 1.52 and 1.62 W/(m·K). The thermal conductivity measured by soil samples differs slightly among the three regions.

Table 5. Deviation of laboratory measurements of thermal conductivity in boreholes.

Hydrogeological Setting	Borehole	Min (W/(m·K))	Max (W/(m·K))	Standard Deviation	Mean (W/(m·K))
Piedmont plain (I)	BD-1	1.32	1.92	0.75	1.53
	BD-2	1.34	2.03	0.89	1.57
	SJZ-1	1.39	1.92	0.62	1.70
	SJZ-2	1.28	1.97	0.79	1.77
	SJZ-3	1.49	2.11	0.81	1.79
Central plain (II)	RQ-1	1.33	1.8	0.32	1.58
	HJ-1	1.34	1.84	0.56	1.54
	HJ-2	1.35	1.95	0.54	1.64
	WQ-1	1.33	1.95	0.44	1.54
	HS-1	1.42	1.75	0.16	1.57
Coastal plain (III)	CZ-1	1.37	1.77	0.21	1.57
	CZ-2	1.26	1.79	0.32	1.59
	HH-1	1.26	1.95	0.69	1.62
	QX-1	1.26	1.88	0.50	1.52
	QX-2	1.14	1.78	0.62	1.52

3.3. TRT by Typical Borehole Configurations

In this study, the BHE was first tested under conditions without heating and cooling for about 20–48 h. When a steady state was reached, the mean fluid temperature was considered the undisturbed ground temperature. Figure 5a shows the inlet and outlet fluid temperature series during the first stage in HS-1. Based on the measured data, both the inlet and outlet temperature decrease rapidly in the first 10 h and remain almost stable during the next 10 to 38 h. However, both inlet and outlet fluid temperatures fluctuated with the outside air temperature variations. This phenomenon also exists in the other 14 boreholes, indicating that insulating the pipes is not sufficient to accurately estimate the ground temperature, and this method produces a certain amount of measuring error. The average inlet and outlet fluid temperature ($T_{\text{in-out-average}}$) of the 15 boreholes in the first phase of the TRT are listed in Table 6.

Table 6. Comparison of undisturbed ground temperature based on TRT measurements and temperature logging.

Hydrogeological Setting	Borehole	$T_{\text{in-out-average}}$ (°C)	$T_{\text{depth-average}}$ (°C)	Absolute Deviation (%)
Piedmont plain (I)	BD-1	16.07	14.85	8.22
	BD-2	16.29	14.91	9.26
	SJZ-1	16.84	/	/
	SJZ-2	16.09	13.98	15.09
	SJZ-3	16.33	14.93	9.38
Central plain (II)	RQ-1	15.24	14.96	1.87
	HJ-1	15.82	/	/
	HJ-2	15.17	15.88	0.71
	WQ-1	15.45	15.71	0.26
	HS-1	17.28	/	/
Coastal plain (III)	CZ-1	16.20	/	/
	CZ-2	15.95	/	/
	HH-1	15.31	14.31	1.00
	QX-1	15.92	15.21	0.71
	QX-2	15.71	/	/

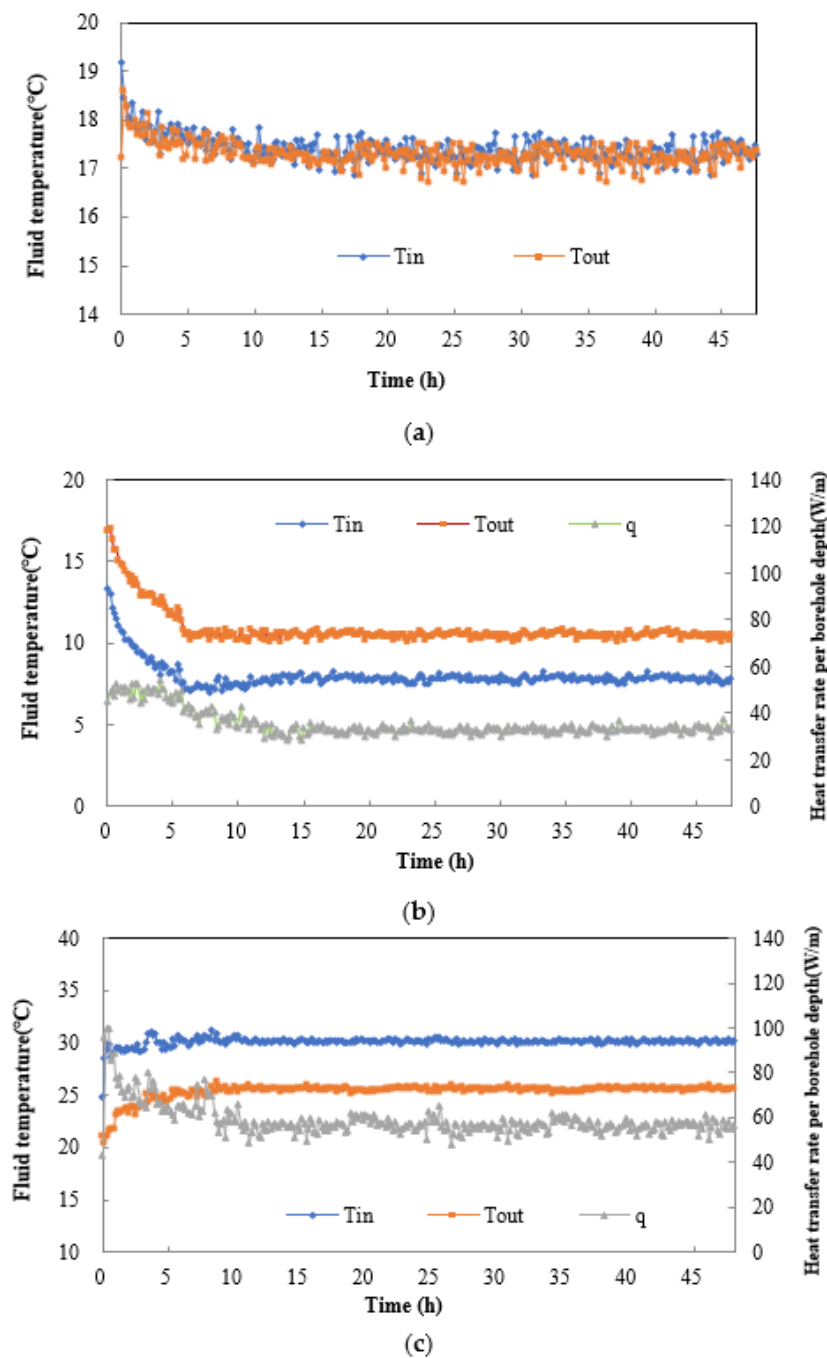


Figure 5. Experimental results under typical heat operation conditions with HS-1: (a) without heating or cooling; (b) heat extraction (T_{in} : 7.83 °C); and (c) heat injection (T_{in} : 30.20 °C).

At the same time, a depth-average temperature ($T_{\text{depth-average}}$), which is also treated as the undisturbed ground temperature, can be obtained from the ground temperature logging of the nine boreholes listed in Section 3.1. These results were then compared with the average inlet and outlet temperature ($T_{\text{in-out-average}}$) produced by the first phase of the TRT shown in Table 6.

In an idealized system, the inlet and outlet fluid temperatures would remain constant over time and consistent with the depth-averaged ground temperature because no external heat is being added to the system. However, there are biases in the results obtained by these two methods with absolute deviation ranging from 0.26% to 15.09%. The difference between the TRT method and the temperature sensor method is not only related to the

accuracy of the measurement equipment but is also influenced by the air temperature, highlighting the importance of both the pipe and test rig insulation during the TRT [21].

After the first phase, a total of 24 TRTs for the 15 boreholes with one or two heat-extraction/injection modes were performed using CHTM. The inlet fluid temperatures for these modes were set as 5–10 °C and 19–33 °C, respectively, and detailed information is listed in Table 3.

Figure 5 shows the experimental measurements under one heat-extraction and heat-injection operation condition in HS-1 with mean flow rates around 1.07 m³/h. Results show that the heat transfer rate of the BHE dropped rapidly as the heating or cooling time increased during the first 12 h. However, the heat transfer rate tended to be steady after 12 h.

The heat-transfer rate was evaluated according to the series data under different operation conditions. Taking HS-1 as an example, when the inlet/outlet fluid temperature of the BHE was 7.83/10.50 °C for the heat-extraction mode, the experimental heat transfer rate of the BHE was 32.81 W/m. When the inlet/outlet temperature of the BHE was 30.19/25.62 °C for the heat-injection mode, the experimental heat transfer rate of the BHE was 56.58 W/m. Figure 6 shows the linear relationship fitted by the regression between the mean fluid temperature T_f and the steady state heat transfer rate of BHEs q . In the present work, the line slope K was 4.8255. The ground thermal conductivity was then obtained based on the parameter estimation method introduced in Section 2.3. In the case of HS-1, this value was 1.50 ± 0.05 W/(m·K).

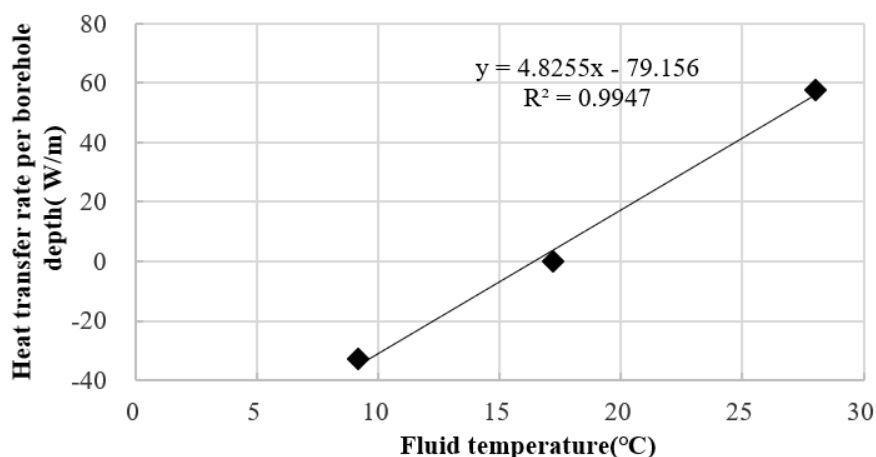


Figure 6. Variation in the heat transfer rate of the BHE with the average fluid temperature.

3.4. Comparison of Thermal Conductivity by CHTM-Based TRT and Laboratory Measurements

Following the same method, the effective thermal conductivity of the other 14 boreholes was calculated. The results are shown in Table 7. A higher effective thermal conductivity was determined in BD and SJZ of the piedmont plain with value ranges between 2.37 and 2.68 W/(m·K). The lower value was reported in boreholes of the central plain with values ranging between 1.35 and 1.63 W/(m·K). Results of other boreholes in the coastal plain range between 1.58 and 1.94 W/(m·K). As mentioned in Sections 2.1 and 3.1, the groundwater flow velocity in the piedmont plain was from 0.013 to 0.26 m/d, while in the central and coastal plain it was from 0.002 to 0.10 m/d. The existence of groundwater flow has a significant effect on the temperature profile of the aquifer [46] and the thermal performance of the BHE will be enhanced as a result of groundwater convection. The large difference in groundwater flow velocity in these regions could be the main factor contributing to the difference in thermal conductivity.

Table 7. The results of in situ thermal conductivity and laboratory methods of 15 boreholes.

Hydrogeological Setting	Borehole	Effective Thermal Conductivity (W/(m·K))		
		TRT	Laboratory Method	Absolute Difference
Piedmont plain (I)	BD-1	2.63	1.57	1.06
	BD-2	2.58	1.53	1.05
	SJZ-1	2.37	1.69	0.68
	SJZ-2	2.63	1.76	0.87
	SJZ-3	2.68	1.79	0.89
Central plain (II)	RQ-1	1.35	1.57	0.22
	HJ-1	1.47	1.54	0.07
	HJ-2	1.63	1.64	0.01
	WQ-1	1.35	1.54	0.19
	HS-1	1.50	1.57	0.07
Coastal plain (III)	CZ-1	1.69	1.60	0.09
	CZ-2	1.58	1.62	0.04
	HH-1	1.70	1.62	0.08
	QX-1	1.94	1.52	0.42
	QX-2	1.61	1.52	0.09

The laboratory mean thermal conductivity of each borehole was obtained by the arithmetic mean method as indicated in Table 5. The results were then compared with those of the CHTM-based TRT of the effective thermal conductivity shown in Table 7.

A bigger difference in the TRT thermal conductivity and laboratory methods occurred in the piedmont plain and the difference ranges between 0.68 and 1.06 W/(m·K). However, boreholes in the central plain exhibit similar results by these two methods. The largest absolute difference is 0.22 W/(m·K) and the smallest is only 0.01 W/(m·K). Most boreholes in the coastal plain exhibit similar results too, and the absolute difference is less than 0.09 W/(m·K), except borehole QX-1.

Although the thermal conductivity by laboratory method is affected by the characteristic of the sediment, there is little difference among these three hydrogeological zones. The results of the TRT are strongly affected by groundwater flow, which shows obvious zonation with hydrogeological conditions. Therefore, the difference between the laboratory and TRT is ultimately influenced by both sediment composition and groundwater flow, though mainly groundwater flow.

In the actual process of estimating thermal conductivity, it is not necessary to apply both methods considering the cost. Therefore, for the central and coastal plain with a relatively homogenous ground, shallow groundwater table, and low groundwater flow velocity, either method for estimating thermal conductivity is reasonable. For the piedmont plain with heterogeneous lithology and high flow velocity of the groundwater, the TRT is highly recommended, and the obtained effective ground thermal conductivity can be a reasonable representation of the geothermal properties.

4. Conclusions

In this paper, ground temperature profiles and ground thermal conductivity for a piedmont alluvial plain, a central alluvial plain, and a coastal plain in the central NCP are investigated. Fifteen boreholes with depths of 100–150 m depth were drilled according to the local hydrogeological settings. Ground temperature profiles were measured through borehole logging. The thermo-physical parameters of drilling cores were measured in a laboratory. Moreover, double U-pipe BHEs were installed and CHTM-based TRTs were implemented to estimate the thermal properties in these boreholes.

Based on the vertical distribution of ground temperature in the three regions in central NCP, the profiles of ground temperature within 150 m in depth can be divided into three sections. The upper one, 10–15 m below the ground surface, is highly influenced by seasonal atmospheric conditions. The middle section, between 15 m and 40 m in depth,

has a relatively constant ground temperature, and the deep section, below 40 m in depth, shows an obvious significant geothermal gradient ranging from 0.018 °C/m to 0.029 °C/m.

Thermal conductivity depends not only on particle size but also on groundwater flow. The laboratory measurements show that the thermal conductivity in the central NCP has an average thermal conductivity varying between 1.52 and 1.79 W/(m·K), with a standard deviation varying between 0.16 and 0.89. Thermal conductivity in the piedmont plain exhibits a larger variability than that of the central and coastal plain due to the significant heterogeneity of lithology. Based on the CHTM-based TRT method, the ground thermal conductivity is found to range between 2.37 and 2.68 W/(m·K) in the piedmont plain and varies between 1.35 and 1.94 W/(m·K) in the central and coastal plains. This finding shows that the piedmont plain has a higher potential for geothermal energy exploitation compared to the central and coastal plains.

Considering effective thermal conductivity, the thermal conductivity estimated by the TRT was similar to the laboratory measurements in the central and coastal plains. A great deviation was detected between the TRT and lab measurements in the piedmont plain due to the presence of groundwater flow. This is because the groundwater flow affects the TRT outputs which in turn increase the effective thermal conductivity. Conclusively, both the TRT and laboratory approaches are proper methods for estimating thermal conductivity in the central and coastal plains due to their relatively homogeneous ground composition and low groundwater flow. In the piedmont, the TRT is highly recommended to estimate the effective thermal conductivity and hydraulic conditions needing to be determined for GSHP system designs in terms of long-term operation.

Author Contributions: W.W. and F.L. designed and performed the experiments and measurements. W.W., C.L. and G.W. implemented the methodology and analyzed the results. All authors provided technical and theoretical support. W.W. and C.L. wrote the manuscript. All authors have read and agreed to the published version of the manuscript.

Funding: This research was funded by the National Key R&D Program of China (Grant no. 2021YFB1507302, 2021YFB1507300), the National Natural Science Foundation of China (Grant no. 41302189), and the China Geological Survey Project (Grant no. DD20221676).

Conflicts of Interest: The authors declare no conflict of interest.

References

1. Zeng, H.; Diao, N.; Fang, Z. Heat transfer analysis of boreholes in vertical ground heat exchangers. *Int. J. Heat Mass Transf.* **2003**, *46*, 4467–4481. [[CrossRef](#)]
2. Blum, P.; Campillo, G.; Münch, W.; Kölbl, T. CO₂ savings of ground source heat pump systems—A regional analysis. *Renew. Energy* **2010**, *35*, 122–127. [[CrossRef](#)]
3. Zhu, J.; Hu, K.; Lu, X.; Huang, X.; Liu, K.; Wu, X. A review of geothermal energy resources, development, and applications in China: Current status and prospects. *Energy* **2015**, *93*, 466–483. [[CrossRef](#)]
4. Lunda, J.W.; Toth, A.N. Direct utilization of geothermal energy 2020 worldwide review. *Geothermics* **2021**, *90*, 101915. [[CrossRef](#)]
5. Wang, W.; Wang, G.; Zhu, X.; Liu, Z. Characteristics and potential of shallow geothermal resources in provincial capital cities of China. *Geology* **2017**, *44*, 1062–1073.
6. Tao, S.; Ru, M.Y.; Du, W.; Zhu, X.; Zhong, Q.R.; Li, B.G.; Shen, G.F.; Pan, X.L.; Meng, W.J.; Chen, Y.L.; et al. Quantifying the rural residential energy transition in China from 1992 to 2012 through a representative national survey. *Nat. Energy* **2018**, *3*, 567–573. [[CrossRef](#)]
7. Wang, H.; Liu, B.; Yang, F.; Liu, F. Test investigation of operation performance of novel split-type ground source heat pump systems for clean heating of rural households in North China. *Renew. Energy* **2021**, *163*, 188–197. [[CrossRef](#)]
8. Cui, P.; Yang, H.; Fang, Z. Heat transfer analysis of ground heat exchangers with inclined boreholes. *Appl. Therm. Eng.* **2006**, *26*, 1169–1175. [[CrossRef](#)]
9. Ouzzane, M.; Eslami-Nejad, P.; Badache, M.; Aidoun, Z. New correlations for the prediction of the undisturbed ground temperature. *Geothermics* **2015**, *53*, 379–384. [[CrossRef](#)]
10. Pouloupatis, P.D.; Tassou, S.A.; Christodoulides, P.; Florides, G.A. Parametric analysis of the factors affecting the efficiency of ground heat exchangers and design application aspects in Cyprus. *Renew. Energy* **2017**, *103*, 721–728. [[CrossRef](#)]
11. Loveridge, F.; Holmes, G.; Powrie, W.; Roberts, T. Thermal response testing through the Chalk aquifer in London, UK. *Proc. Inst. Civ. Eng. Geotech. Eng.* **2013**, *166*, 197–210. [[CrossRef](#)]

12. Barry-Macaulay, D.; Bouazza, A.; Singh, R.M.; Wang, B.; Ranjith, P.G. Thermal conductivity of soils and rocks from the Melbourne (Australia) region. *Eng. Geol.* **2013**, *164*, 131–138. [[CrossRef](#)]
13. Luo, J.; Rohn, J.; Xiang, W.; Bertermann, D.; Blum, P. A review of ground investigations for ground source heat pump (GSHP) systems. *Energy Build.* **2016**, *117*, 160–175. [[CrossRef](#)]
14. Dalla Santa, G.; Galgaro, A.; Sassi, R.; Cultrera, M.; Scotton, P.; Mueller, J.; Bertermann, D.; Mendrinos, D.; Pasquali, R.; Perego, R.; et al. An updated ground thermal properties database for GSHP applications. *Geothermics* **2020**, *85*, 101758. [[CrossRef](#)]
15. Tarnawski, V.R.; Momose, T.; Leong, W.H.; Bovesecchi, G.; Coppa, P. Thermal Conductivity of Standard Sands. Part I. Dry-State Conditions. *Int. J. Thermophys.* **2009**, *30*, 949–968. [[CrossRef](#)]
16. Abu-Hamdeh, N.H. Thermal Properties of Soils as affected by Density and Water Content. *Biosyst. Eng.* **2003**, *86*, 97–102. [[CrossRef](#)]
17. Zhu, X.; Gao, Z.; Chen, T.; Wang, W.; Lu, C.; Zhang, Q. Study on the Thermophysical Properties and Influencing Factors of Regional Surface Shallow Rock and Soil in China. *Front. Earth Sci.* **2022**, *10*, 864548. [[CrossRef](#)]
18. Zhang, Y.; Gao, P.; Yu, Z.; Fang, J.; Li, C. Characteristics of ground thermal properties in Harbin, China. *Energy Build.* **2014**, *69*, 251–259. [[CrossRef](#)]
19. Luo, J.; Luo, Z.; Xie, J.; Xia, D.; Huang, W.; Shao, H.; Xiang, W.; Rohn, J. Investigation of shallow geothermal potentials for different types of ground source heat pump systems (GSHP) of Wuhan city in China. *Renew. Energy* **2018**, *118*, 230–244. [[CrossRef](#)]
20. Spitler, J.D.; Gehlin, S.E.A. Thermal response testing for ground source heat pump systems—An historical review. *Renew. Sustain. Energy Rev.* **2015**, *50*, 1125–1137. [[CrossRef](#)]
21. Radioti, G.; Sartor, K.; Charlier, R.; Dewallef, P.; Nguyen, F. Effect of undisturbed ground temperature on the design of closed-loop geothermal systems: A case study in a semi-urban environment. *Appl. Energy* **2017**, *200*, 89–105. [[CrossRef](#)]
22. Hu, J.Z. An improved analytical model for vertical borehole ground heat exchanger with multiple-layer substrates and groundwater flow. *Appl. Energy* **2017**, *202*, 537–549. [[CrossRef](#)]
23. Franco, A.; Conti, P. Clearing a path for ground heat exchange systems: A review on thermal response test (TRT) methods and a geotechnical routine test for estimating soil thermal properties. *Energies* **2020**, *13*, 2965. [[CrossRef](#)]
24. Fujii, H.; Okubo, H.; Nishi, K.; Itoi, R.; Ohyama, K.; Shibata, K. An improved thermal response test for U-tube ground heat exchanger based on optical fiber thermometers. *Geothermics* **2009**, *38*, 399–406. [[CrossRef](#)]
25. Poppei, J.; Schwarz, R.; Peron, H.; Mattsson, N.; Laloui, L.; Wagner, R.; Rohner, E. *Innovative Improvements of Thermal Response Tests (Intermediate Report)*; Swiss Federal Office of Energy: Berne, Switzerland, 2006.
26. Wang, H.; Qi, C.; Du, H.; Gu, J. Improved method and case study of thermal response test for borehole heat exchangers of ground source heat pump system. *Renew. Energy* **2010**, *35*, 727–733. [[CrossRef](#)]
27. Wang, H.; Qi, C.; Du, H.; Gu, J. Thermal performance of borehole heat exchanger under groundwater flow: A case study from Baoding. *Energy Build.* **2009**, *41*, 1368–1373. [[CrossRef](#)]
28. Cao, G.; Han, D.; Currell, M.J.; Zheng, C. Revised conceptualization of the North China Basin groundwater flow system: Groundwater age, heat and flow simulations. *J. Asian Earth Sci.* **2016**, *127*, 119–136. [[CrossRef](#)]
29. Zongyu, C.; Jixiang, Q.; Jianming, X.; Jiaming, X.; Hao, Y.; Yunju, N. Paleoclimatic interpretation of the past 30 ka from isotopic studies of the deep confined aquifer of the North China plain. *Appl. Geochem.* **2003**, *18*, 997–1009. [[CrossRef](#)]
30. Foster, S.; Garduno, H.; Evans, R.; Olson, D.; Tian, Y.; Zhang, W.; Han, Z. Quaternary Aquifer of the North China Plain—Assessing and achieving groundwater resource sustainability. *Hydrogeol. J.* **2004**, *12*, 81–93. [[CrossRef](#)]
31. Shu, Y.; Villholth, K.G.; Jensen, K.H.; Stisen, S.; Lei, Y. Integrated hydrological modeling of the North China Plain: Options for sustainable groundwater use in the alluvial plain of Mt. Taihang. *J. Hydrol.* **2012**, *464–465*, 79–93. [[CrossRef](#)]
32. Wang, Y.; Chen, Z.; Duan, B.; Shao, J. Experimental evidence for hyperfiltration of saline water through compacted clay aquitard in the Hebei Plain. *J. Earth Sci.* **2014**, *25*, 1076–1082. [[CrossRef](#)]
33. Li, X.; Zhou, A.; Gan, Y.; Yu, T.; Wang, D.; Liu, Y. Controls on the $\delta^{34}\text{S}$ and $\delta^{18}\text{O}$ of dissolved sulfate in the Quaternary aquifers of the North China Plain. *J. Hydrol.* **2011**, *400*, 312–322. [[CrossRef](#)]
34. Chen, W.H. *Groundwater in Hebei*; Seismological Press: Beijing, China, 1999.
35. Zhang, Z.J.; Fei, Y.H. *Atlas of Groundwater Sustainable Utilization in North China Plain*; Sinomaps Press: Beijing, China, 2009.
36. Xing, L.; Guo, H.; Zhan, Y. Groundwater hydrochemical characteristics and processes along flow paths in the North China Plain. *J. Asian Earth Sci.* **2013**, *70–71*, 250–264. [[CrossRef](#)]
37. Lu, X.; Jin, M.; van Genuchten, M.T.; Wang, B. Groundwater recharge at five representative sites in the Hebei Plain, China. *Ground Water* **2011**, *49*, 286–294. [[CrossRef](#)]
38. Li, J.; Zhou, H.; Qian, K.; Xie, X.; Xue, X.; Yang, Y.; Wang, Y. Fluoride and iodine enrichment in groundwater of North China Plain: Evidences from speciation analysis and geochemical modeling. *Sci. Total Environ.* **2017**, *598*, 239–248. [[CrossRef](#)]
39. Kharazmi, A.; Faraji, N.; Hussin, R.M.; Saion, E.; Yunus, W.M.; Behzad, K. Structural, optical, opto-thermal and thermal properties of ZnS-PVA nanofluids synthesized through a radiolytic approach. *Beilstein. J. Nanotechnol.* **2015**, *6*, 529–536. [[CrossRef](#)]
40. Eskilson, P.; Claesson, J. Simulation Model for Thermally Interacting Heat Extraction Boreholes. *Numer. Heat Transf.* **1988**, *13*, 149–165. [[CrossRef](#)]
41. Lamarche, L.; Beauchamp, B. A new contribution to the finite line-source model for geothermal boreholes. *Energy Build.* **2007**, *39*, 188–198. [[CrossRef](#)]

42. Badache, M.; Eslami-Nejad, P.; Ouzzane, M.; Eslami-Nejad, P.; Badache, M.; Aidoun, Z.; Lamarche, L. A new modeling approach for improved ground temperature profile determination. *Renew. Energy* **2016**, *85*, 436–444. [[CrossRef](#)]
43. Popiel, C.O.; Wojtkowiak, J.; Biernacka, B. Measurement of temperature distribution in ground. *Exp. Therm. Fluid Sci.* **2001**, *25*, 301–309. [[CrossRef](#)]
44. van Manen, S.M.; Wallin, E. Ground temperature profiles and thermal rock properties at Wairakei, New Zealand. *Renew. Energy* **2012**, *43*, 313–321. [[CrossRef](#)]
45. Xiong, Z.; Fisher, D.E.; Spitler, J.D. Development and validation of a Slinky™ ground heat exchanger model. *Appl. Energy* **2015**, *141*, 57–69. [[CrossRef](#)]
46. Luo, J.; Huang, W.; Zhu, Y.; Jiao, Y.; Xiang, W.; Rohn, J. Influence of groundwater levels on effective thermal conductivity of the ground and heat transfer rate of borehole heat exchangers. *Appl. Therm. Eng.* **2018**, *128*, 508–516. [[CrossRef](#)]